Review

Adsorption Factors in Enhanced Coal Bed Methane Recovery: A Review

Theodora Noely Tambaria [1,2,*], **Yuichi Sugai** [1] **and Ronald Nguele** [1]

[1] Department of Earth Resources Engineering, Kyushu University, 744 Motooka, Nishiku, Fukuoka 819-0395, Japan; sugai@mine.kyushu-u.ac.jp (Y.S.); nguele@mine.kyushu-u.ac.jp (R.N.)

[2] Department of Geological Engineering, Universitas Gadjah Mada, Yogyakarta 55281, Indonesia

* Correspondence: theodora.noely.t@mail.ugm.ac.id

Abstract: Enhanced coal bed methane recovery using gas injection can provide increased methane extraction depending on the characteristics of the coal and the gas that is used. Accurate prediction of the extent of gas adsorption by coal are therefore important. Both experimental methods and modeling have been used to assess gas adsorption and its effects, including volumetric and gravimetric techniques, as well as the Ono–Kondo model and other numerical simulations. Thermodynamic parameters may be used to model adsorption on coal surfaces while adsorption isotherms can be used to predict adsorption on coal pores. In addition, density functional theory and grand canonical Monte Carlo methods may be employed. Complementary analytical techniques include Fourier transform infrared, Raman spectroscopy, XR diffraction, and ^{13}C nuclear magnetic resonance spectroscopy. This review summarizes the cutting-edge research concerning the adsorption of CO_2, N_2, or mixture gas onto coal surfaces and into coal pores based on both experimental studies and simulations.

Keywords: ECBM; gas adsorption; coal

1. Introduction

Coal bed methane (CBM) has been extracted from coal seams for many years [1]. This methane is held in micropores [2] and so numerous methods have been developed based on gas injection techniques to remove the maximum possible amount of methane from these micropores. CBM relied on the natural pressure in the coal bed, but these methods were unable to achieve complete extraction [3]. Since then, other technologies have been developed, including the use of polymers, water injection, and proppant injection [4–10]. Among the various method, gas injection has been found to provide maximum methane recovery of up to 90% [11]. The gases commonly used in enhanced CBM (ECBM) recovery are carbon dioxide (CO_2) and nitrogen (N_2) or and mixture of the two [12–15].

The extraction process comprises gas injection into the CBM reservoir, followed by the selective adsorption of the gas on the coal surfaces and in the coal pores, methane desorption from the coal matrix, and methane flow along fractures in the bed based on Darcy's Law [16–20] (Figure 1). Both the gas injection and adsorption rates in the coal bed are critical because these factors affect the coal structure and thus the extent of methane recovery [18,21–23]. Based on accurate adsorption analyses, including factors such as bed swelling and permeability, the effectiveness of ECBM extraction can be predicted [18,24]. Accurate predictions of gas adsorption must also take into account the possibility of sequestration of the injected gas [17]. Despite that the publication of many research and review articles on the subject of gas adsorption on coal, the adsorption of gases by coal beds based on actual coal pore morphologies and chemical structures poorly understood [25,26].

This review discusses the state of research developments regarding gas adsorption on coal surfaces and pores using experimental and simulation methods following the injection of CO_2, N_2, or CO_2-N_2. Present knowledge regarding methane generation on coal, coal gas adsorption characteristics and ECBM recovery is examined. The review concludes with a summary and prospects for future research.
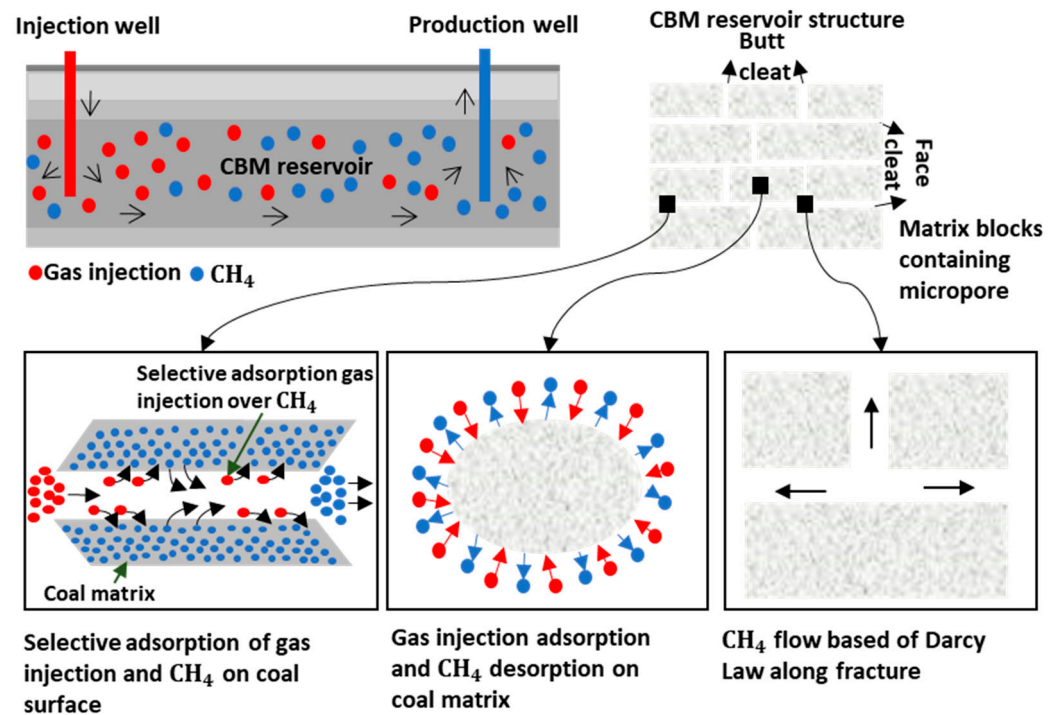
Figure 1. The ECBM extraction process based on gas injection. Adapted from [16–20].

2. Methane in Coal

Methane is present in coal beds both as an adsorbed gas (accounting for 80–90% of the entire methane content in a coal seam) and a free gas [16]. The latter can be compressed in pore spaces, condensed as a solid or liquid, dissolved in the coal structure or adsorbed on surfaces [2]. Coal contains methane gas because of biogenic and thermogenic processes [27] that occur during coalification with resultant storage of the gas in the coal seams [19].

Biogenic methane produced by bacterial activity at shallow to moderate depths (<500 m) [2,28,29] begins with fragmentation of the coal macromolecules via two main processes; exfoliation and/or anaerobic oxidation [30]. The biogenic processes begin with oxygen consumption after which biologically-generated CO_2 is converted to methane [29]. The anaerobic oxidation reactions are promoted by various bacterial species capable of oxidizing aromatic and aliphatic structures to CO_2 [30]. The majority of the biogenic methane and CO_2 generated in this manner are most likely dissolved in water and removed from the system during compaction and coalification [31].

The thermogenic formation of CBM results from kerogen or the cracking of heavier hydrocarbons and increases with depth [32]. Thermogenic processes that occur in deep coal [33] at higher pressures increase the coverage of the coal surface by the CBM and result in stronger interactions between adsorbate molecules [34]. Although the composition of coal bed gases does not have a strong relationship with either coal rank or depth, thermogenic generation usually begins in highly volatile bituminous rank coal and increases with rank [32]. The thermogenic processes cause coals with higher ranks to have greater holding capacities such that they retain more gas, and also yield micropores that act as methane reservoir [30,35–37].

CBM can be produced at almost any time during the coal life cycle based on methanogenic bacterial growth in response to heating if the coal is uplifted and favorable subsurface environmental conditions are restored [30]. Secondary biogenic gases are also generated through bacterial metabolic activity based in the introduction of bacteria by meteoric waters migrating through permeable coal beds [31]. The biological methane in coal be continuously produced, although thermogenic gases tends to result in higher total gas contents in coal beds compared with pure biogenic-derived gases [30].

3. Gas Adsorption Characteristic of Coal

Gas adsorption on coal is influenced by the specific characteristics of the coal. Research has confirmed the effects of the coal condition and the type of coal, as well as the moisture content, ash yield, maceral content and coal pore distribution on the efficiency of ECBM extraction.

3.1. Effects of Sample Condition

The sample aspect that has most frequently been shown to affect coal gas adsorption tests is particle size. Specifically bulk samples adsorb gases more slowly than crushed coal samples [38,39]. The crushed coal used for adsorption analyses is typically in the size range of 100–60 mesh [38,40–42] while bulk coal specimen are usually approximately 2 cm cubes [40]. The crushed coal has a higher diffusivity and requires a shorter measurement time to achieve equilibrium compared with coal blocks [39,43,44].

Even so, crushed coal has several detrimental effects on adsorption. As an example, this material will have a damaged pore network in which closed pores have been opened. Therefore, the sample surface area will have been increased so that the adsorption capacity is artificially improved compared with the original state [38]. The crushing of coal also decreases the moisture level and increases the amount of adsorbed gas [40]. When crushed coal is used, it is nearly impossible to observe coal shrinkage or swelling because of adsorption, in contrast to trials using solid coal [45].

3.2. Moisture Effects

Moisture is an important factor in adsorption because water molecules are highly polar [46], and so can modify, the gas adsorption kinetics, mechanisms and capacity [43,46–50]. A comparison of adsorption during ECBM extraction trial using moist and dry coals has shown that dry conditions provide the highest gas adsorption capacity and saturation values [51]. This occurs because the adsorption sites that were originally occupied by moisture become available for methane adsorption [49,52–54].

Dry coal has greater coal gas adsorption capacity but can yield a large correction factor because coal in the field contains natural moisture [47,55]. Natural (or inherent) moisture affects the methane adsorption capacity differently for each coal rank. Specifically, low-rank coals exhibit greater capacities for water retention medium-rank coals show pore-blockage and fewer micropores as a result of water adsorption which limits the gas adsorption capacities and high-rank coals contain numerous in micropores that provide sufficient pore space for the exchange of water and methane [49].

3.3. Ash Yield Effects

Ash yield is attributed to pore infilling, blockage cleats and fracture systems resulting from extraneous mineral matter (such as clays and carbonates) in coal [56]. The adsorption capacity of coal is decreased with increases in the mineral ash content [57] because this material reduces the storage capacity [53] and blocks gas migration [38]. The presence of mineral matter indicates that the increasing pore volume, especially in open pores and macropores, such that gas adsorption is inhibited at faster desorption rates [2,58,59]. For these reasons, coal having a high ash yield is generally not suitable for ECBM recovery with gas injection because it cannot absorb the injected gas or requires the application of high pressures and temperatures for adsorption [60].

3.4. Maceral Effects

In coal, organic matter is known as the maceral component and this material affects gas adsorption and absorption [41]. Generally, the feasibility of performing ECBM recovery is based on assessing the vitrinite content of coal [17].

Vitrinite is a type of maceral that affects the pore structure of the coals [61], especially the coal micropores and pore distribution [62]. A higher vitrinite content leads to a higher void volume [63], greater specific surface area (SSA) [45], increased adsorption capacity [56],

and decreased desorption rate [2,53,64]. Coal that is rich in vitrinite also reacts more effectively to CO_2 injection and undergoes swelling [65,66].

Liptinite is another type of maceral that affects the mesopores in coal [62]. By encouraging surface diffusion, liptinite can promote the adsorption of CO_2 and also act as a medium for gas transport by adsorbing CO_2 while acting as a catalyst [65]. Inertinite differs from vitrinite and liptinite that it contains more macropores and fewer micropores [67]. As a result of the dominance of macropores in this material, liptinite lower the apparent surface area of the coal [62], resulting in a shorter time being required to achieve equilibrium [68], and producing significant swelling upon CO_2 injection [66].

3.5. Coal Pore Effects

Methane in coal is stored on the walls of micropore networks [2] an various methods are used to understand the manner in which gases can be extracted from these micropores. ECBM recovery research has demonstrated that these pores modify the adsorption and flow of gases that are injected into coal or other porous media [69,70].

The pore volume in coal is determined by its thermal maturity [71] such that increasing maturity increases the adsorption capacity [2]. Figure 2 presents pore size distribution curves for coals from low rank to high rank as obtained from nuclear magnetic resonance (NMR) analyses [72].
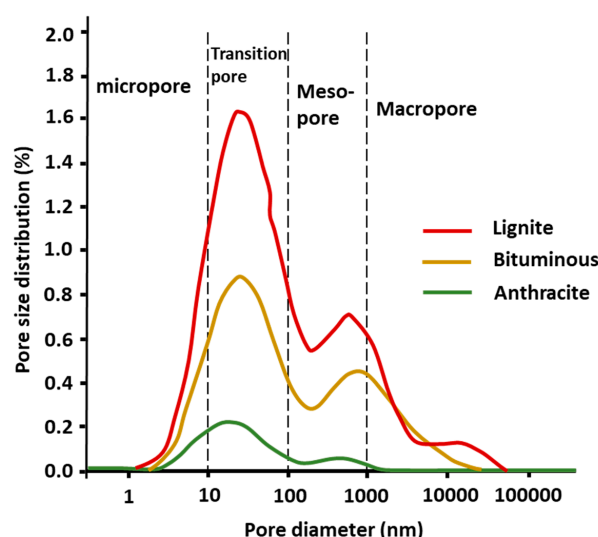
Figure 2. Pore distributions in different coal ranks as determined using an NMR method. Modified from [72].

Low-rank coal contains primary epigenetic pores having irregular shapes and poor connectivity. Although the dehydration of lignite to low-rank coal reduces the moisture and oxygen-to-carbon ratio of the material [36], low-rank coal exhibit a high degree of porosity and low pore compressibility [14].

Metamorphism changes pores into circular, oval or slit morphologies [73,74] and medium-rank coal contains pore sizes ranging from macropores to micropores [75]. Medium-rank coal with a high proportion of micropores is the most suitable for industrial methane production [73].

High-rank coals contain primarily micropores with limited pore connectivity as a result the coalification process [49,62]. Coalification also leads to smaller coal pore, larger surface areas, a greater number of micropores and a higher methane content [52,76,77]. Although increases in coal rank are associated with increases in the methane content [78], the pores gradually close and form flattened structure that make gas absorption impossible [35,37,62]. As a result of the small pore surfaces, gas injection into high-rank coal must be performed at high pressures [79].

4. Gas Injection for ECBM Recovery

As noted, CO_2, N_2 and their mixtures are commonly used for ECBM extraction, and the injection of pure or mixed gas will lead to different adsorption effect, as explained in this section.

4.1. CO₂ Injection

CO_2 is an acidic gas [80] that is widely for ECBM recovery because it can extract methane with significant efficiency [12]. Coal has a high adsorption affinity for CO_2 and so this gas is adsorbed rapidly, whereupon it seeps into micropores [47,64,65,81–84]. The CO_2 molecule also has a small kinetic diameter and so can replace methane originally present in the micropores [12,14,85]. However, the CO_2 storage capacity is affected by temperature and pressure, both of which can change the coal structure and permeability [35,43,86–90].

4.2. N₂ Injection

N_2 is used for ECBM extraction because N_2 promotes methane desorption from the coal matrix [12,14,91,92]. N_2 reaches equilibrium quickly, leading to a more rapid response [91,93]. N_2 adsorption increases with increases in pressure, although, N_2 undergoes weak interactions with adsorbents [94,95]. N_2 injection also alters the coal pore structure and increases the transition pore volume such that the pore volume, pore size distribution, and connectivity are all increased [96].

4.3. Mixed Gas (CO₂-N₂) Injection

ECBM recovery experiments using gas mixtures have been carried out, Such mixtures have been found to be applicable to low-permeability coal [13,97] because N_2 prevents expansion of the coal matrix and increases the diffusion coefficient to provide faster methane extraction [14]. However, such mixtures are not suitable for carbon sequestration [98].

The desorption of methane is enhanced in the case that the mixed gas has a CO_2 concentration of less than 10%. Increasing the proportion of CO_2 increases the probability of adsorption while decreasing the desorption of methane [99]. The adsorption selectivity obtainable from a mixed gas injection may be calculated as [99]

$$S_{CO_2/N_2} = \frac{\left(x_{CO_2}/x_{N_2}\right)_{adsorbed}}{\left(y_{CO_2}/y_{N_2}\right)_{bulk}}, \tag{1}$$

where S_{CO_2/N_2} is the adsorption selectivity and, x and y represent the mole fractions of each gas in the adsorbed and bulk phase, respectively. An adsorption selectivity of 1 indicates that N_2 is adsorbed more strongly than CO_2 while a value greater than 1 indicates the opposite.

5. Gas Adsorption

Temperature and pressure are important factors in ECBM recovery. Higher temperatures lead to reduced gas adsorption capacities, reductions in the residual forces on the coal matrix surface and breaking of the bonds between gas molecules and the coal [92]. In contrast, higher pressures increase the coal adsorption capacity [100]. A higher pressure increases the adsorbate density and provides greater surface coverage and stronger interactions of the adsorbate molecules with the coal [34]. Thus, increasing the temperature is detrimental because this promotes gas desorption rather than adsorption [101]. The present section describes calculations, isotherms and thermodynamic parameters associated with gas adsorption on coal, and discusses modeling used to predict gas adsorption in coal pores.

5.1. Adsorption Calculations

In most cases, coal injection calculations are performed using volumetric and gravimetric methods [102]. However, each method has a different calculation focus and considerations that are affected by the adsorption isotherm. In particular, experimental methods

take into account both excess and absolute adsorption with the difference between the two being required to determine the adsorbed phase density [26].

5.1.1. Volumetric Methods

The volumetric/manometric methods are techniques for assessing adsorption based on variations in the pressure of the adsorbate gas in a coal sample [26,55,103,104] (Figure 3). The associated equation is [104]

$$\Delta n^{ex} = \left(\frac{P\Delta V}{ZRT}\right)_{pump} - \left(\frac{PV_{void}}{ZRT}\right)_{sample\ cell}, \tag{2}$$

where n^{ex} is the Gibbs excess adsorption (mmol g^{-1}), P is the pressure (MPa), ΔV is the gas volume that is injected(cm^3), V_{void} is the void volume (cm^3), R is the ideal gas constant (8.314 J mol^{-1} K^{-1}), Z is the compressibility factor of the gas, and T is the temperature (K). The value of Z is calculated using the equation [92]

$$Z = 1 + \left(0.083 - \frac{0.422}{T_r^{1.6}}\right)\frac{P_r}{T_r} + \omega\left(0.139 - \frac{0.172}{T_r^{4.2}}\right)\frac{P_r}{T_r}, \tag{3}$$

where ω is the acentric factor for the gas, P_r is the reduced pressure (MPa), and T_r is the reduced temperature (K). P_r and T_r are, respectively, expressed as [92]

$$P_r = \frac{P}{P_c}, \tag{4}$$

$$T_r = \frac{T}{T_c}, \tag{5}$$

The critical pressure (P_c) value for CO_2 and N_2 are 7.39 MPa and 3.395 MPa, respectively while the critical temperature (T_c) values are 304.2 K and 126 K. The acentric factors (ω) for CO_2 and N_2 are 0.224 and 0.040, respectively.
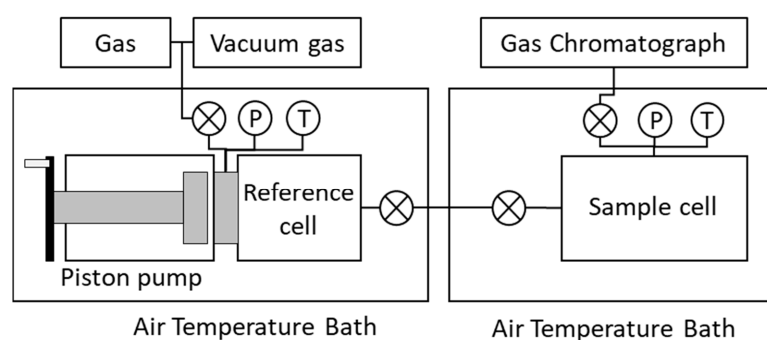

Figure 3. A diagram showing the apparatus used during adsorption analysis based on a volumetric method. Modified after [104].

5.1.2. Gravimetric Methods

The gravimetric methods are based on the use a microbalance [102] to monitor changes in sample mass during gas adsorption [26,103] (Figure 4). The equation is [26]

$$n^{ex} = \Delta m + \frac{m_s}{\rho_s}\rho_{gas}, \tag{6}$$

where n^{ex} is the Gibbs excess adsorption (mmol/g), Δm is the mass change (g), m_s is the coal sample mass, ρ_s is the density of the coal sample (g cm^{-3}), and ρ_{gas} is the density of the gas (g cm^{-3}).
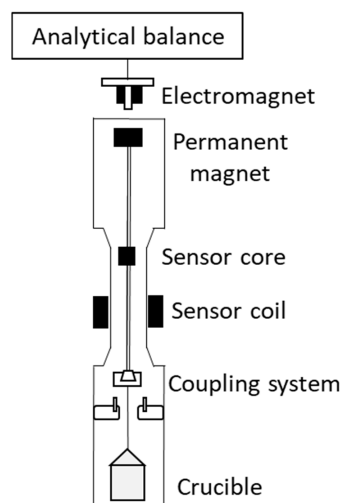
Figure 4. Diagram of the apparatus used for gravimetric adsorption methods. Modified after [105].

5.2. Modeling for the Prediction of Coal Adsorption

Predictions of coal adsorption have been performed using many mathematical models, with the Ono–Kondo lattice model being commonly used, in addition to numerical simulations. The Ono–Kondo process estimates adsorption on the microscopic scale by considering thermodynamic equilibrium in multilayer adsorption based on the equation [106]

$$n_{ex} = \rho_b \left(\frac{2n_0'(1 - \exp(\varepsilon_{is}/k'T))}{\rho_{mc}} \frac{1}{\frac{\rho_b}{\rho_{mc} - \rho_b} + \exp(\varepsilon_{is}/k'T)} \right), \tag{7}$$

where n_{ex} is the amount of absolute adsorption (mmol g^{-1}), ρ_b is the bulk density (g cm^{-3}), ρ_{mc} is the adsorbed phase density at maximum capacity (g cm^{-3}) n_0' is the extent of monolayer adsorption (mmol g^{-1}), k' is Boltzmann's constant, 1.38×10^{-23} (J mol^{-1} K^{-1}), and ε_{is} is the interaction energy between the adsorbate molecules and the adsorbent surface (kJ mol^{-1}).

Numerical simulations are used to calculate value within a bidisperse model system using computer codes that describe gas transport during adsorption in coal macropores and micropores. The relevant equations are [83]

$$\frac{\partial}{\partial t}(\phi_a \rho_a) = \frac{1}{r_a^2} \frac{\partial}{\partial r_a} \left(\phi_a D_a r_a^2 \frac{\partial \rho_a}{\partial r_a} \right) + \frac{3(1 - \phi_a)\phi_i D_i}{R_i} \frac{\partial \rho_i}{\partial r_i} \bigg|_{r_i = R_i}, \tag{8}$$

$$\frac{\partial}{\partial t}[\phi_i \rho_i + (1 - \phi_i)q] = \frac{1}{r_i^2} \frac{\partial}{\partial r_i} \left(\phi_i D_i r_i^2 \frac{\partial \rho_i}{\partial r_i} \right), \tag{9}$$

where ϕ is the adsorbate-wall interaction potential in a micropore (J), ρ is the gas phase density (kmol m^{-3}), r is the pore radius (m), D is the gas diffusivity (m^{2}s^{-1}), q is the adsorbate concentration (kmol m^{-3}) and the subscripts a and i indicate macropores and micropores, respectively.

5.3. Thermodynamic Parameters

Adsorption on coal surfaces can be understood based on thermodynamic parameters, such as the isosteric heat of adsorption (Q_{st}), change in entropy (ΔS), change in enthalpy (ΔH), change in Gibbs free energy (ΔG) and surface potential (Ω) [107]. The isosteric heat parameter can also be used to assess the degree of surface homogeneity [108].

Q_{st} resulting from the interaction between an absorbent and adsorbate, can be calculated as [109]

$$Q_{st} = RT^2 \left(\frac{\partial \ln P}{\partial T} \right)_V, \tag{10}$$

where R is the ideal gas constant (J mol^{-1} K^{-1}), T is the temperature (K), P is pressure (MPa) and V is the amount of gas adsorption as determined by the Langmuir method (cm^3 g^{-1}).

The energy released from the adsorbate attaching to the adsorbent surface, otherwise known as the surface potential (Ω) can be determined as [101]

$$\Omega = -RT \int_0^P \frac{V}{P} \, dP, \tag{11}$$

where R is the ideal gas constant (J mol^{-1} K^{-1}), T is the temperature (K), P is the pressure (MPa) and V is the amount of gas adsorption determined by the Langmuir method (cm^3 g^{-1}).

The Gibbs free energy (ΔG) is an indicator of the reaction spontaneity and is calculated as [101]

$$\Delta G = \frac{\Omega}{V}, \tag{12}$$

where Ω is the surface potential and V is the amount of gas adsorption determined by the Langmuir method (cm^3 g^{-1}).

The change in entropy (ΔS) is a measure of the variation in order at the gas-solid interface on the coal surface and can be written as [107]

$$\Delta S = \frac{\Delta H - \Delta G}{T}, \tag{13}$$

where ΔH is the energy change associated with the adsorption process ($\Delta H = -Q_{st}$), ΔG is the change in Gibbs free energy, and T is the temperature (K).

It is evident that adsorption on the coal surface is affected by temperature, pressure and pore size distribution. Increasing the temperature decreases the isosteric heat of adsorption [101] while increasing the equilibrium pressure reduces the change in entropy and surface potential [101]. A pore system in the coal in which micropores are dominant will be indicated by higher Ω, ΔG and ΔS values [107].

5.4. Adsorption Isotherms

Adsorption isotherms provide information related to physical adsorption at equilibrium pressure. The most commonly used methods for analyzing adsorption isotherms obtained from coal are the Langmuir, Brunauer–Emmett–Teller (BET), Dubinin–Radushkevich (DR), and Dubinin–Astakhov (DA) techniques. These four methods each assess different types of adsorption and different types of curves. Specifically, the Langmuir D-A and D-R approaches are used with type I isotherms, whereas the BET method is used with type II isotherms [110] (Figure 5). Type I isotherms reflect increased adsorption and pore filling, whereas type II isotherms indicate multilayer physical adsorption [111].

5.4.1. Langmuir Method

The Langmuir method is based on dynamic equilibrium and the result of Langmuir is used conjunction with type I isotherms [110]. This technique produces results similar to experimental data [56] because the Langmuir pressure typically decreases with increases in moisture content [50] and coal rank [53]. The adsorption used in this method calculation is [112]

$$V = \frac{V_L P}{P_L + P}, \tag{14}$$

where P is the equilibrium gas or vapor pressure (MPa), V is the gas adsorption amount (cm^3 g^{-1}), V_L is the Langmuir monolayer volume constant (cm^3 g^{-1}), and P_L is the Langmuir pressure at half of V_L (MPa). The weakness of the Langmuir model is that it only applies to monolayer adsorption on solid surfaces [113,114].

5.4.2. BET Method

The BET method is used to obtain information regarding multilayers based on as type II isotherms [110]. This technique expands the concept of the Langmuir adsorption isotherm by assuming perfect multilayer adsorption via the formation of monolayers [115]. The BET data are obtained by injecting N_2 gas at 77 K into a coal sample and provide information related to the type of pores in which adsorption occurs, the SSA of the material and the total pore volume [37,62,74,96,116,117]. The BET method is also used to calculate the SSA values of mesoporous solids in general [77,118]. The pore types determined from this technique are classified as H1, H2 or H3. The H1 pores promote adsorption whereas the H2 and H3 types are better for desorption and diffusion [74]. The BET equation used to calculate adsorption is [110]

$$\frac{1}{V\left(\frac{P_0}{P} - 1\right)} = \frac{1}{V_m C} + \frac{C - 1}{V_m C}\left(\frac{P}{P_0}\right),$$ (15)

where P is the pressure (MPa), V_a is the volume of gas adsorbed ($cm^3 g^{-1}$), P/P_0 is the relative pressure, V_m is the volume of adsorbate as a monolayer ($cm^3 g^{-1}$) and C is a constant related to the net heat of adsorption.

5.4.3. Dubinin Method

The Dubinin method assumes that the adsorbates molecules fill the micropores [110] and the relevant data are obtained by injecting gaseous CO_2 at 273 K into a coal sample [119]. This technique uses the D-R equation to analyze micropore capacity and surface area along with the D-A equation compute the pore size distribution [120]. Isotherm equations based on the Dubinin method have been found to reproduce experimental data better than either monolayer or multilayer pore filling models. The relevant equations are [110]

For the D-R method,

$$W = W_0 \exp\left[-\left(\frac{RT}{\beta E}\ln\frac{P_0}{P}\right)^2\right],$$ (16)

For the D-A method

$$W = W_0 \exp\left[-\left(\frac{RT}{\beta E}\ln\frac{P_0}{P}\right)^n\right],$$ (17)

where W is the pore volume filled at P/P_0 ($cm^3\ g^{-1}$), W_0 is the total volume of the micropore system ($cm^3\ g^{-1}$), β is the sorbate affinity coefficient ($mol^2\ kJ^{-2}$), E_0 is the characteristic energy ($kJ\ mol^{-1}$), R is the ideal gas constant ($J\ mol^{-1}\ K^{-1}$) and T is the temperature (K), and P_0/P is the inverse of the relative pressure of the adsorbate.
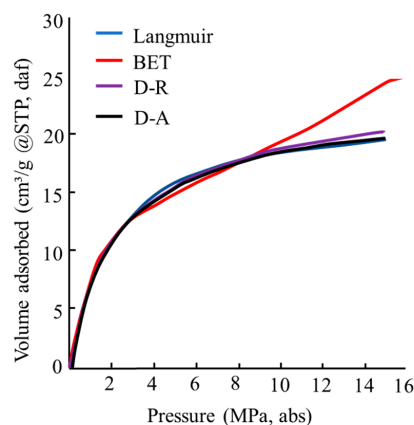

Figure 5. Adsorption isotherm curves based on the Langmuir, BET, D-R and D-A methods. Adapted from [110].

5.5. Modeling for Predicting Gas Adsorption in Coal Pores

Density functional theory (DFT) is often used to produce models for predicting gas adsorption in coal pores, while the grand canonical Monte Carlo (GCMC) method is employed to simulate adsorption isotherm.

5.5.1. DFT

DFT models can be used to determine the size distributions of micro-, meso-, and macropores, as well as pore structure morphologies [16,121]. DFT is able to calculate a pore size distribution (PSD) based on the use of different adsorbates such as N_2 at 77.4 K and CO_2 at 273 K with CO_2 being more suitable [121]. In the case of narrow micro- and mesopores, DFT methods provide more accurate pore size analysis [122]. This process involves two steps. Initially, a kernel is produced to determine the PSD from test data for use as a reference for subsequent calculation, after which PSD is obtained an integral adsorption equation corresponds to the kernel. This equation is [16,123]

$$N(p/p_0) = \int_{\text{Dmin}}^{\text{Dmax}} N(p/p_0, D) f(D) dD,$$ (18)

where $N(p/p_0)$ is the number of moles adsorbed at pressure P, D is the pore size (nm), $N(p/p_0, D)$ is the kernel obtained from theoretical isotherms with different pore widths and $f(D)$ is the PSD of the heterogeneous solid adsorbent.

Using the DFT method, factors such as the adsorption energy (E_a), formation energy (E_f) and cohesive energy (E_c) can be calculated as follows [109].

$$E_a = E_{AB} - E_A - E_B,$$ (19)

$$E_f = \left(E_{sample} - n_c \mu_c \right) / N,$$ (20)

$$E_c = \left(E_{sample} - n_c E_c \right) / N,$$ (21)

where E_{AB}, E_A, and E_B are the energies of the AB complex (eV) and the A and B isolates, E_{sample} is the energy of the coal sample complex (eV), n_c is the moles of carbon atoms (mol), μ_c is the chemical potential of the carbon atoms (eV mol^{-1}), and N is the total number of atoms in the coal sample.

5.5.2. GCMC

Using the GCMC method, the chemical potential can be calculated as [124]

$$\mu = \mu^0 + RT \ln\left(\frac{\phi P}{p^0}\right),$$ (22)

where μ is the chemical potential, p^0 is the standard pressure, μ^0 is the chemical potential, P is the gas reservoir pressure and ϕ is the fugacity coefficient.

The first step in calculating gas adsorption using the GCMC approach is modeling the movement of a gas molecule, followed by the generation and then deletion of a gas molecule. The relevant equations are [125]

$$P_m = \min\left[1, \exp\left(\frac{-\Delta\varphi}{kT}\right)\right],$$ (23)

$$P_p = \min\left[1, \frac{V}{\lambda^3(N+1)} \exp\frac{\mu - \Delta\varphi}{kT}\right],$$ (24)

$$P_d = \min\left[1, \frac{\lambda^3 N}{V} \exp\left(\frac{-\mu - \Delta\varphi}{kT}\right)\right],$$ (25)

where P_m is the pressure of movement (MPa), P_p is the pressure of generation (MPa), P_d is the pressure of deletion (MPa), N is the number of gas molecules, $\Delta\varphi$ is the change in the total potential energy of the system after one of the three steps (J), k is the Boltzmann constant (JK^{-1}), λ is the wavelength (nm), and V is the volume (nm^3).

These simulation are repeated until equilibrium is achieved after a number of deletion and insertion steps [124]. Based on these GCMC simulations and experimental data, gas adsorption can be calculated using the equation [126]:

$$N_{excess} = N_{abs} - N_A P V_f / RT, \tag{26}$$

where N_{excess} is the excess adsorption amount, N_{abs} is the absolute adsorption amount, N_A is the Avogadro constant, P is the pressure (Pa), V_f is the free volume, R is the ideal gas constant (J/mol K) and T is the temperature (K).

5.6. Adsorption into the Coal Chemical Structure

Modern techniques, such as Fourier transform infrared (FTIR) Raman, and ^{13}C NMR spectroscopies as well as X-ray diffraction have been applied to the analysis of coal [99]. Low-rank coals have been determined to be primarily composed of oxygen-containing functional groups [49] while medium-rank coals with lower volatile matter content exhibit a high degree of aromatization and lower amount of oxygen-containing functional and aliphatic compounds [127]. High-rank coals contain some oxygen-based functional groups [49].

^{13}C NMR can be used to elucidate the macro-molecular structure of coal [99]. Such studies have indicated that lignite exhibits decarboxylation and dehydration, bituminous coals show decarboxylation and hydrogen disproportionation and anthracite contains aromatic rings and shows dehydrogenization (Figure 6). The ^{13}C NMR is data can be processed using the equation [99].

$$X_{BP} = \frac{f_a^B}{f_a^H + f_a^P + f_a^S} \tag{27}$$

where X_{BP} is the average degree of aromatic ring condensation in the coal structure, f_a^H is the protonated aromatic carbon, f_a^P is the oxygen-linked aromaticity carbon, f_a^S is the side branch aromaticity carbon, and f_a^B is the bridging aromaticity carbon.
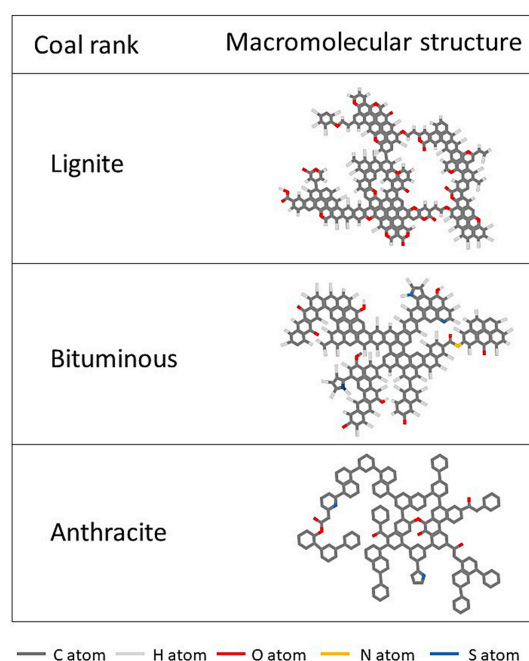

Figure 6. The macromolecular structure of a variety of coal ranks. Modified from [99].

FTIR is used to analyze the functional groups of organic compounds, including aromatic, oxygen-containing, aliphatic, and hydroxyl structures [92,127]. Prior to such analyses, the coal sample should be demineralized [127] and CO_2 will generate a peak at 2330 cm^{-1} [128]. Results from FTIR studies of CO_2 adsorption on wet coal indicated a significant decline in CO_2 adsorption capacity compared with dry samples, although aliphatic and aromatic functional groups were unaffected [92] (Figure 7).
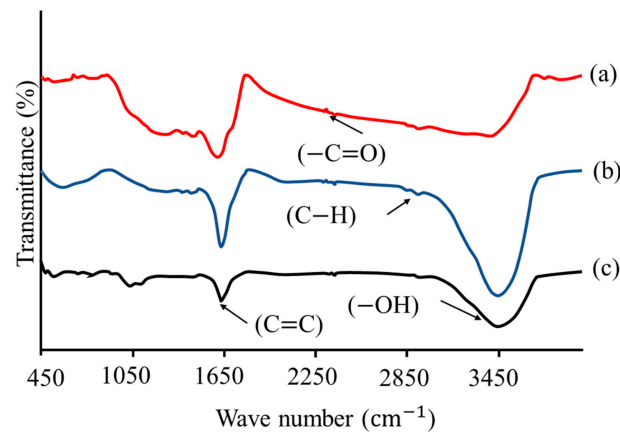

Figure 7. FTIR spectra of (**a**) wet coal exposed to CO_2 at 300K and pressure up to 6 MPa, (**b**) dry coal exposed to CO_2 at 300 K, and (**c**) fresh coal. Modified from [92].

The Raman method allows the analysis of microcrystalline carbon structure [127] based on signal related to the vibrations of aromatic fused rings [129]. This technique can be used to study gas adsorption coal by evaluating the D peak (1332 to 1366 cm^{-1}) and G peak (1576 to 1608 cm^{-1}) [127].

According to [128], coal must be demineralized prior to evaluating gas adsorption using XRD and the difference between treated and untreated coal following gas injection can be clearly seen at the $2\theta = 23°$ peak position [128] (Figure 8). The (002) band is the most prominent band in the XRD diffractogram, and change in the position of this peak are related to changes in the aromatic sheet structure (that is, in the interlayer spacing d_{002}) [128,130]. The equations for calculating the interlayer spacing between the aromatic sheets (d_{002}) and the average crystallite stacking height (*Lc*) are [128]

$$d_{002} = \lambda / 2 \sin \theta_{002}, \tag{28}$$

$$L_c = 0.9\lambda / \beta_{002} \cos \theta_{002}, \tag{29}$$

where λ is the X-ray wavelength (Å), θ_{002} is the 002 diffraction angle, β_{002} is the width at half maximum intensity of the pure reflection profile in radians.
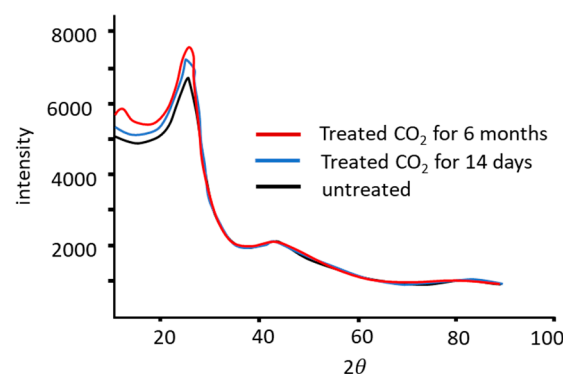

Figure 8. The XRD pattern obtained from untreated coal and coal treated CO_2 for different time spans. The primary difference is at $2\theta = 23°$. Modified from [128].

6. Adsorption Effects

Previous research has shown that CO_2 injection is likely to produce swelling of coal [26,93,131,132], whereas N_2 injection is less likely to do so [131,132]. The effect of gas can be assessed using volumetric and gravimetric method and by monitoring tri-axial stress (Table 1). Additional measurement devices, such as strain gauges, strain bridges, linear variable differential transformers (LVDT), and optical analyzers, can be used to assess instantaneous volume changes [102]. Compared with non-pressurized methods, pressure-based techniques can show initial fracturing and tend to indicate higher gas release volumes [133]. Increases in the adsorption pressure promote expansion of the coal matrix that in turn reduces the cleat apertures and closes pre-existing fractures [39,134–137]. These phenomena decrease the permeability of the coal and inhibit methane production [24,118].

Table 1. Summary of experimental studies related to gas adsorption by coal. Sg: strain gauge, Sb: strain bridges, L: LVDT, O: optical and P_{max}: maximum experimental pressure.

Coal Rank	Coal Sample	Adsorbate	Experimental Method		Experimental Analysis		Swelling Result	Reference
			Sorption	Swelling	P_{max}	T		
Bituminous	Block	CO_2	Gravimetric	O	16 MPa	55 °C	1.8%	[138]
Semi-anthracite	Block	CO_2/N_2	Manometric/ volumetric	Sg	16 MPa	318–338 K	1.42%	[43]
Bituminous	Cube	CO_2	Volumetric	Sg	6 MPa	30 °C	3.8×10 μE	[51]
Anthracite	Core	CO_2	Volumetric	L and Sg	18 MPa	45 °C	0.9%	[139]
High volatile bituminous	Block	CO_2	Tri-axial	Sg	0.4 MPa	25 °C	1200 μE	[140]
Bituminous	core	CO_2	Adsorption deformation testing system	Sg	2.5 MPa	Room	1.8%	[137]

7. Discussion and Prospects for Future Research

Experimental work and simulations methods aimed at understanding gas adsorption during ECBM recovery are being increasingly improved. This review focused on the effects of the chemical structure of coal, taking into account various properties of the coal and the injection gas. Gas adsorption is essentially a solid-liquid system in which adsorption leads to the infusion of a sorbate into a sorbent, which is converted to a rubbery state such that its pores disappear [128]. As a consequence, moisture is an important factor in the adsorption of gas by coal. Experimental data shows that the adsorption by dry coal has higher adsorption capacity than wet coal [49,52–54]. Analyze of the chemical structures of coals have established that interactions between hydroxyl and carboxyl functional groups with water molecules are stronger than those with gas molecules [92]. Hence, dry coal will always exhibit higher gas adsorption capacity than wet coal, even though wet coal is the closest to the natural condition of this material.

Demineralized coal is commonly used in coal structural analyses but does not closely match real coal. The various minerals in coal can be dissolved and mobilized during gas adsorption [141] and so a challenge for future research will be to ascertain the effects of mineral content on gas adsorption by coal.

The maceral content of coal and its pore size have a unique correlation. The maceral content is greatly affected by the deposition of coal, whereas pore size is affected by the coalification process. Studies of gas adsorption by coal using FTIR spectroscopy have demonstrated that coal with a higher vitrinite content generates higher adsorption capacity because the small pores of the vitrinite are able to capture gas molecules [142]. Adsorption isotherm analyses using the Langmuir, Dubinin and BET methods will all show differences in the effects of pores in coal. The Langmuir technique assumes monolayer formation,

while the BET method postulates the formation of multilayers based on monolayers and the Dubinin calculations are predicated on pore filling. The most significant difference between the Langmuir and BET methods is that the former takes each adsorption site into account but assumes only one molecule at each site, while the BET method calculates the adsorption of several molecules at each site [115]. Adsorption analyses using the BET method indicate minimal variations in the mesopore volume between dry and wet coal [92]. However, the micropore surface area is increased in dry coal and decreased in wet coal [92]. The Dubinin method is better at fitting experimental data than the monolayer or multilayer pore filling models. Differences in pore size and correlations in these differences with coal chemical structures can be examined using XRD by investigating the structural geometry in micropores [128]. Overall, the data show that a higher vitrinite content and more accessible pores promotes gas adsorption and methane desorption from the coal matrix.

The gas that is injected during ECBM recovery depends on the type of coal being processed. Coal having a higher oxygen content will adsorb CO_2 and N_2 more strongly because the heat of adsorption of these gases will be higher [99]. Thermodynamic calculations also indicate that CO_2 adsorbs to the coal surfaces more readily than N_2 and is more stable once adsorbed [101]. The fraction of the coal surface populated by CO_2 molecules increases with increases in the heat of CO_2 adsorption, indicating higher CO_2 adsorption [128]. Both simulations and experimental data regarding adsorption selectivity associated with injecting CO_2-N_2 mixtures show similar trends in which CO_2 is preferentially adsorbed and lower rank coal has higher adsorption selectivity [99] (Figure 9). However, even though CO_2 is preferentially adsorbed increasing the percentage of CO_2 in the gas mixture makes it more difficult to desorb methane [99]. This phenomenon occurs because CO_2 alters the coal pore sizes via internal and external expansion effects [137]. The injection of pure CO_2 also results in swelling of the coal such that methane extraction is inhibited. Thus, for the purpose of ECBM recovery, the injection of CO_2-N_2 mixtures is the best option.
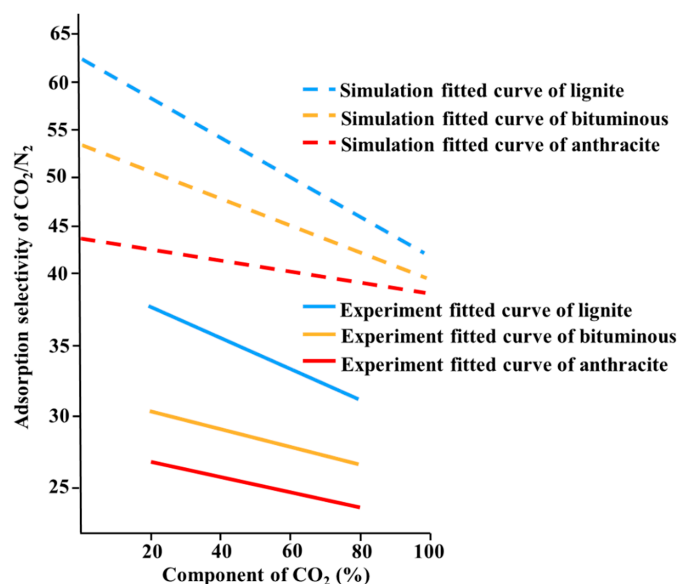

Figure 9. Adsorption selectivity during CO_2/N_2 injection into lignite, bituminous and anthracite based on simulations and experimental work. A selectivity value larger than 1 indicates preferential adsorption of CO_2. Modified from [99].

Laboratory experiments using volumetric and gravimetric methods are commonly used to assess gas adsorption by coal. The volumetric methods determine gas adsorption at a variety of pressures but cannot assess variations in volume and density after adsorption [26]. The gravimetric methods are highly accurate but have several weaknesses. Specifically, these techniques require buoyancy correction [102] and make it difficult to

control the sample temperature during the experiment [26]. As a consequence of these issues, modeling should be used to improve accuracy.

Modeling-based predictions of gas adsorption have been found to be similar to experimental data, although these models tend to neglect physical adsorption mechanisms. Even though the Ono–Kondo lattice model considers the crystalline coal structure, this technique assumes monolayer adsorption and omits swelling of the coal matrix [106]. Numerical simulations provide better predictions but assume uniform micropores [83]. DFT and GCMC provide improved results. DFT can predict a variety of coal pore sizes while GCMC simulates adsorption based on gas molecule movement, generation, and deletion on coal.

Various methods proposed to understand the adsorption in chemical structures have their respective advantages and disadvantages (Table 2). The ^{13}C NMR detects total aromaticity better than other methods and XRD explains a better aromatic layer than method [143]. The coalification process affects gas adsorption in coal and increasing proportions of aromatic components is related to increasing vitrinite reflectance value [127]. Aliphatic and aromatic in coal are unaffected by water molecules because these groups are hydrophobic [92].

Table 2. Advantages and disadvantages of different techniques for evaluating gas adsorption in the chemical structures of coal.

Method	Advantages	Disadvantages	Source
^{13}C NMR	Detect aromatic CO_2 adsorption in different coal types and coal ranks in detail	It is difficult to describe complexity of selectivity gas adsorption	[144]
FTIR	Changes in the amounts of functional groups can be detected, and the evolution of micropore structure can be described	Discovered the inconsistencies in functional groups for the same type of coal	[145–147]
Raman	Consider the loss of oxygen groups in aromatics	It shows higher average lateral size of crystalline aromatics in coal compared to the XRD result	[143,148]
XRD	It shows an accurate change in micropore by interplanar spacing, stacking height and lateral size	Cannot directly mention destruction in later spacing of the microcrystalline aromatic by adsorption or by other mechanisms	[149]

Even though adsorption measurement methods have been improved, there have been few reports related to the use of these techniques to study the injection of mixed gases into coal. This suggests opportunities for future research in this field as a means of examining ECBM by injecting a variety of gases into different coal ranks. An improved understanding of the adsorption processes and more detailed data should allow more accurate simulations of ECBM recovery.

8. Conclusions

This review examined various aspects of gas adsorption by coal during ECBM extraction. The most important factors as affecting this process are follows:

- Moisture

Experimental data show that adsorption is inhibited on wet coal because the adsorption sites are occupied by water molecules. This effect is reinforced by interactions between water molecules and hydroxyl/ carboxyl functional groups in the coal.

- Maceral and pore size

Changes in the coal structural geometry related to the presence of mesopores and micropores as well as chemical structure can affect the extent of gas adsorption in coal pores. The presence of maceral is determined by the type of coal deposit while pore sizes are affected by the coalification process, and these relationships indicate that higher vitrinite proportions and more accessible pores increase the possibility of gas adsorption.

- Gas characteristics

CO_2 is adsorbed by coal to a greater extent than N_2, although the injection of CO_2 alone results in swelling of the coal. The use of CO_2-N_2 mixture appears to be the best option for ECBM recovery.

- Cutting-edge methods used to understand adsorption

Laboratory experiments using volumetric and gravimetric methods can provide approximate information concerning gas adsorption by coal. However, such experiments also require modeling to ensure accuracy, such as the Ono–Kondo lattice model or numerical simulations. Since such modeling does not take physical mechanisms into account, DFT and GCMC method may also be applied. Analytical techniques including ^{13}C NMR and XRD can also monitor gas adsorption and may provide superior data.

Further research concerning gas adsorption by coal as a means of improving ECBM extraction is required, especially concerning the injection of mixed gases into a variety of coal ranks.

References

1. Alexis, D.A.; Karpyn, Z.T.; Ertekin, T.; Crandall, D. Fracture permeability and relative permeability of coal and their dependence on stress conditions. *J. Unconv. Oil Gas Resour.* **2015**, *10*, 1–10. [CrossRef]
2. Crosdale, P.J.; Beamish, B.; Valix, M. Coalbed methane sorption related to coal composition. *Int. J. Coal Geol.* **1998**, *35*, 147–158. [CrossRef]
3. Wang, R.; Zhang, N.; Liu, X.; Wu, X.; Chen, J.; Ma, L. Characteristics of Pore Volume Distribution and Methane Adsorption on Shales. *Adsorpt. Sci. Technol.* **2015**, *33*, 915–938. [CrossRef]
4. Bae, J.-S.; Bhatia, S.K.; Rudolph, V.; Massarotto, P. Pore Accessibility of Methane and Carbon Dioxide in Coals. *Energy Fuels* **2009**, *23*, 3319–3327. [CrossRef]
5. Lu, T.; Yu, H.; Zhou, T.; Mao, J.; Guo, B. Improvement of methane drainage in high gassy coal seam using waterjet technique. *Int. J. Coal Geol.* **2009**, *79*, 40–48. [CrossRef]
6. Keshavarz, A.; Badalyan, A.; Carageorgos, T.; Bedrikovetsky, P.; Johnson, R. Stimulation of coal seam permeability by micro-sized graded proppant placement using selective fluid properties. *Fuel* **2015**, *144*, 228–236. [CrossRef]
7. Umezaki, T.; Kawamura, T.; Okamoto, K.; Hattori, A.; Kobayashi, Y. Swelling properties and coefficient of permeability of friction-reducing polymer for pull-out of temporary sheet piles. *Soils Found.* **2018**, *58*, 797–807. [CrossRef]
8. Ahamed, M.; Perera, M.; Dong-Yin, L.; Ranjith, P.; Matthai, S. Proppant damage mechanisms in coal seam reservoirs during the hydraulic fracturing process: A review. *Fuel* **2019**, *253*, 615–629. [CrossRef]
9. Lyu, S.; Wang, S.; Chen, X.; Shah, S.; Li, R.; Xiao, Y.; Dong, Q.; Gu, Y. Experimental study of a degradable polymer drilling fluid system for coalbed methane well. *J. Pet. Sci. Eng.* **2019**, *178*, 678–690. [CrossRef]
10. Li, Z.; Wei, G.; Liang, R.; Shi, P.; Wen, H.; Zhou, W. LCO2-ECBM technology for preventing coal and gas outburst: Integrated effect of permeability improvement and gas displacement. *Fuel* **2021**, *285*, 119219. [CrossRef]
11. Zarrouk, S.J.; Moore, T. Preliminary reservoir model of enhanced coalbed methane (ECBM) in a subbituminous coal seam, Huntly Coalfield, New Zealand. *Int. J. Coal Geol.* **2009**, *77*, 153–161. [CrossRef]

12. Shimada, S.; Li, H.; Oshima, Y.; Adachi, K. Displacement behavior of CH4 adsorbed on coals by injecting pure CO_2, N_2, and CO_2–N_2 mixture. *Environ. Earth Sci.* **2005**, *49*, 44–52. [CrossRef]

13. Seomoon, H.; Lee, M.; Sung, W. Analysis of methane recovery through CO 2 –N 2 mixed gas injection considering gas diffusion phenomenon in coal seam. *Energy Explor. Exploit.* **2016**, *34*, 661–675. [CrossRef]

14. Oudinot, A.Y.; Riestenberg, D.E.; Koperna, G.J. Enhanced Gas Recovery and CO_2 Storage in Coal Bed Methane Reservoirs with N2 Co-Injection. *Energy Procedia* **2017**, *114*, 5356–5376. [CrossRef]

15. Cho, S.; Kim, S.; Kim, J. Life-cycle energy, cost, and CO_2 emission of CO_2-enhanced coalbed methane (ECBM) recovery framework. *J. Nat. Gas Sci. Eng.* **2019**, *70*, 102953. [CrossRef]

16. Qi, L.; Tang, X.; Wang, Z.; Peng, X. Pore characterization of different types of coal from coal and gas outburst disaster sites using low temperature nitrogen adsorption approach. *Int. J. Min. Sci. Technol.* **2017**, *27*, 371–377. [CrossRef]

17. Godec, M.; Koperna, G.; Gale, J. CO_2-ECBM: A Review of its Status and Global Potential. *Energy Procedia* **2014**, *63*, 5858–5869. [CrossRef]

18. Mukherjee, M.; Misra, S. A review of experimental research on Enhanced Coal Bed Methane (ECBM) recovery via CO_2 sequestration. *Earth-Sci. Rev.* **2018**, *179*, 392–410. [CrossRef]

19. Harpalani, S.; Ouyang, S. A New Laboratory Technique to Estimate Gas Diffusion Characteristics of Coals. In Proceedings of the International Coalbed Methane Symposium, Tuscaloosa, AL, USA, 11–17 June 1999; pp. 141–149.

20. Vishal, V.; Mahanta, B.; Pradhan, S.; Singh, T.; Ranjith, P. Simulation of CO_2 enhanced coalbed methane recovery in Jharia coalfields, India. *Energy* **2018**, *159*, 1185–1194. [CrossRef]

21. Pan, Z.; Connell, L.D. A theoretical model for gas adsorption-induced coal swelling. *Int. J. Coal Geol.* **2007**, *69*, 243–252. [CrossRef]

22. Kim, H.J.; Shi, Y.; He, J.; Lee, H.-H.; Lee, C.-H. Adsorption characteristics of CO_2 and CH4 on dry and wet coal from subcritical to supercritical conditions. *Chem. Eng. J.* **2011**, *171*, 45–53. [CrossRef]

23. Hol, S.; Peach, C.J.; Spiers, C.J. Applied stress reduces the CO_2 sorption capacity of coal. *Int. J. Coal Geol.* **2011**, *85*, 128–142. [CrossRef]

24. Pan, Z.; Connell, L.D. Modelling permeability for coal reservoirs: A review of analytical models and testing data. *Int. J. Coal Geol.* **2012**, *92*, 1–44. [CrossRef]

25. White, C.M.; Smith, D.H.; Jones, K.L.; Goodman, A.L.; Jikich, S.A.; LaCount, R.B.; DuBose, S.B.; Ozdemir, E.; Morsi, A.B.I.; Schroeder, K.T. Sequestration of Carbon Dioxide in Coal with Enhanced Coalbed Methane Recovery—A Review. *Energy Fuels* **2005**, *19*, 659–724. [CrossRef]

26. Busch, A.; Gensterblum, Y. CBM and CO_2-ECBM related sorption processes in coal: A review. *Int. J. Coal Geol.* **2011**, *87*, 49–71. [CrossRef]

27. Susilawati, R.; Esterle, J.S.; Golding, S.D.; Mares, T.E. Microbial Methane Potential for the South Sumatra Basin Coal: Formation Water Screening and Coal Substrate Bioavailability. *Energy Procedia* **2015**, *65*, 282–291. [CrossRef]

28. Saghafi, A. Potential for ECBM and CO_2 storage in mixed gas Australian coals. *Int. J. Coal Geol.* **2010**, *82*, 240–251. [CrossRef]

29. Ahmed, M.; Smith, J. Biogenic methane generation in the degradation of eastern Australian Permian coals. *Org. Geochem.* **2001**, *32*, 809–816. [CrossRef]

30. Moore, T.A. Coalbed methane: A review. *Int. J. Coal Geol.* **2012**, *101*, 36–81. [CrossRef]

31. Scott, A.R.; Kaiser, W.R.; Ayers, W.B. Thermogenic and secondary biogenic gases, San Juan Basin, Colorado and New Mexico—Implications for coalbed gas producibility. *Am. Assoc. Pet. Geol. Bull.* **1994**, *78*, 1186–1209. [CrossRef]

32. Rice, D.D. Composition and Origins of Coalbed Gas. *AAPG Bull.* **1993**, *77*. [CrossRef]

33. Al-Mahmoud, M.J.; Inan, S.; Al-Duaiji, A.A. Coal occurrence in the Jurassic Dhruma Formation in Saudi Arabia: Inferences on its gas and surface mining potential. *Int. J. Coal Geol.* **2014**, *124*, 5–10. [CrossRef]

34. Zheng, Y.; Li, Q.; Yuan, C.; Tao, Q.; Zhao, Y.; Zhang, G.; Liu, J. Influence of temperature on adsorption selectivity: Coal-based activated carbon for CH4 enrichment from coal mine methane. *Powder Technol.* **2019**, *347*, 42–49. [CrossRef]

35. Merkel, A.; Gensterblum, Y.; Krooss, B.; Amann-Hildenbrand, A. Competitive sorption of CH_4, CO_2 and H_2O on natural coals of different rank. *Int. J. Coal Geol.* **2015**, *150–151*, 181–192. [CrossRef]

36. Levine, J.R. Coalification: The Evolution of Coal as a Source Rock and Reservoir Rock for Oil and Gas. In *Hydrocarbon in Coal*; Law, B.E., Rice, D.D., Eds.; American Association of Petroleum Geologists Studies in Geology: Tuscaloosa, AL, USA, 1993; Volume 38, pp. 39–77.

37. Li, Y.; Zhang, C.; Tang, D.; Gan, Q.; Niu, X.; Wang, K.; Shen, R. Coal pore size distributions controlled by the coalification process: An experimental study of coals from the Junggar, Ordos and Qinshui basins in China. *Fuel* **2017**, *206*, 352–363. [CrossRef]

38. Olajossy, A. Some parameters of coal methane system that cause very slow release of methane from virgin coal beds (CBM). *Int. J. Min. Sci. Technol.* **2017**, *27*, 321–326. [CrossRef]

39. Pone, J.D.N.; Halleck, P.M.; Mathews, J.P. Sorption Capacity and Sorption Kinetic Measurements of CO_2 and CH_4 in Confined and Unconfined Bituminous Coal. *Energy Fuels* **2009**, *23*, 4688–4695. [CrossRef]

40. Kim, D.; Seo, Y.; Kim, J.; Han, J.; Lee, Y. Experimental and Simulation Studies on Adsorption and Diffusion Characteristics of Coalbed Methane. *Energies* **2019**, *12*, 3445. [CrossRef]

41. Busch, A.; Krooss, B.; Gensterblum, Y.; van Bergen, F.; Pagnier, H. High-pressure adsorption of methane, carbon dioxideand their mixtures on coals with a special focus on the preferential sorption behaviour. *J. Geochem. Explor.* **2003**, *78–79*, 671–674. [CrossRef]

42. Mastalerz, M.; Gluskoter, H.; Rupp, J. Carbon dioxide and methane sorption in high volatile bituminous coals from Indiana, USA. *Int. J. Coal Geol.* **2004**, *60*, 43–55. [CrossRef]

43. Battistutta, E.; van Hemert, P.; Lutynski, M.; Bruining, H.; Wolf, K.-H. Swelling and sorption experiments on methane, nitrogen and carbon dioxide on dry Selar Cornish coal. *Int. J. Coal Geol.* **2010**, *84*, 39–48. [CrossRef]

44. Ozdemir, E.; I Morsi, B.; Schroeder, K. CO_2 adsorption capacity of argonne premium coals. *Fuel* **2004**, *83*, 1085–1094. [CrossRef]

45. Skoczylas, N.; Pajdak, A.; Młynarczuk, M. CO_2 Adsorption–Desorption Kinetics from the Plane Sheet of Hard Coal and Associated Shrinkage of the Material. *Energies* **2019**, *12*, 4013. [CrossRef]

46. Švábová, M.; Weishauptová, Z.; Přibyl, O. The effect of moisture on the sorption process of CO_2 on coal. *Fuel* **2012**, *92*, 187–196. [CrossRef]

47. Busch, A.; Gensterblum, Y.; Krooss, B.; Littke, R. Methane and carbon dioxide adsorption–diffusion experiments on coal: Upscaling and modeling. *Int. J. Coal Geol.* **2004**, *60*, 151–168. [CrossRef]

48. Crosdale, P.J.; Moore, T.; Mares, T. Influence of moisture content and temperature on methane adsorption isotherm analysis for coals from a low-rank, biogenically-sourced gas reservoir. *Int. J. Coal Geol.* **2008**, *76*, 166–174. [CrossRef]

49. Chen, M.-Y.; Cheng, Y.-P.; Li, H.-R.; Wang, L.; Jin, K.; Dong, J. Impact of inherent moisture on the methane adsorption characteristics of coals with various degrees of metamorphism. *J. Nat. Gas Sci. Eng.* **2018**, *55*, 312–320. [CrossRef]

50. Guo, H.; Cheng, Y.; Wang, L.; Lu, S.; Jin, K. Experimental study on the effect of moisture on low-rank coal adsorption characteristics. *J. Nat. Gas Sci. Eng.* **2015**, *24*, 245–251. [CrossRef]

51. Hao, D.; Zhang, L.; Li, M.; Tu, S.; Zhang, C.; Bai, Q.; Wang, C. Experimental study of the moisture content influence on CH4 adsorption and deformation characteristics of cylindrical bituminous coal core. *Adsorpt. Sci. Technol.* **2018**, *36*, 1512–1537. [CrossRef]

52. Cai, Y.; Liu, D.; Pan, Z.; Yao, Y.; Li, J.; Qiu, Y. Pore structure and its impact on CH4 adsorption capacity and flow capability of bituminous and subbituminous coals from Northeast China. *Fuel* **2013**, *103*, 258–268. [CrossRef]

53. Laxminarayana, C.; Crosdale, P.J. Role of coal type and rank on methane sorption characteristics of Bowen Basin, Australia coals. *Int. J. Coal Geol.* **1999**, *40*, 309–325. [CrossRef]

54. Li, J.; Li, B. Evolution features of coal matrix porosity with the variation in temperature and stress. *IOP Conf. Ser. Mater. Sci. Eng.* **2017**, *191*, 12050. [CrossRef]

55. Siemons, N.; Busch, A. Measurement and interpretation of supercritical CO_2 sorption on various coals. *Int. J. Coal Geol.* **2007**, *69*, 229–242. [CrossRef]

56. Kumar, H.; Mishra, M.K.; Mishra, S. Sorption capacity of Indian coal and its variation with rank parameters. *J. Pet. Explor. Prod. Technol.* **2019**, *9*, 2175–2184. [CrossRef]

57. Yalçin, E.; Durucan, Ş. Methane capacities of Zonguldak coals and the factors affecting methane adsorption. *Min. Sci. Technol.* **1991**, *13*, 215–222. [CrossRef]

58. Faiz, M.M.; Aziz, N.I.; Hutton, A.C.; Jones, B.G. Porosity and gas sorption capacity of some eastern Australian coals in relation to coal rank and composition. *Coalbed Methane Symp.* **1992**, *19*, 9–13.

59. Karayiğit, A.I.; Mastalerz, M.; Oskay, R.G.; Buzkan, I. Bituminous coal seams from underground mines in the Zonguldak Basin (NW Turkey): Insights from mineralogy, coal petrography, Rock-Eval pyrolysis, and meso-and microporosity. *Int. J. Coal Geol.* **2018**, *199*, 91–112. [CrossRef]

60. Fitzgerald, J.; Pan, Z.; Sudibandriyo, M.; Robinson, J.R.; Gasem, K.; Reeves, S. Adsorption of methane, nitrogen, carbon dioxide and their mixtures on wet Tiffany coal. *Fuel* **2005**, *84*, 2351–2363. [CrossRef]

61. Bustin, R.; Clarkson, C. Geological controls on coalbed methane reservoir capacity and gas content. *Int. J. Coal Geol.* **1998**, *38*, 3–26. [CrossRef]

62. Shen, J.; Qin, Y.; Zhao, J. Maceral Contribution to Pore Size Distribution in Anthracite in the South Qinshui Basin. *Energy Fuels* **2019**, *33*, 7234–7243. [CrossRef]

63. Rodrigues, C.F.A.; de Sousa, M.J.L. The measurement of coal porosity with different gases. *Int. J. Coal Geol.* **2002**, *48*, 245–251. [CrossRef]

64. Beamish, B.; Crosdale, P.J. Instantaneous outbursts in underground coal mines: An overview and association with coal type. *Int. J. Coal Geol.* **1998**, *35*, 27–55. [CrossRef]

65. Karacan, C.; Mitchell, G.D. Behavior and effect of different coal microlithotypes during gas transport for carbon dioxide sequestration into coal seams. *Int. J. Coal Geol.* **2003**, *53*, 201–217. [CrossRef]

66. Larsen, J.W. The effects of dissolved CO_2 on coal structure and properties. *Int. J. Coal Geol.* **2004**, *57*, 63–70. [CrossRef]

67. Unsworth, J.F.; Fowler, C.S.; Jones, L.F. Moisture in coal: 2. Maceral effects on pore structure. *Fuel* **1989**, *68*, 18–26. [CrossRef]

68. Keshavarz, A.; Sakurovs, R.; Grigore, M.; Sayyafzadeh, M. Effect of maceral composition and coal rank on gas diffusion in Australian coals. *Int. J. Coal Geol.* **2017**, *173*, 65–75. [CrossRef]

69. Brandani, S.; Mangano, E.; Sarkisov, L. Net, excess and absolute adsorption and adsorption of helium. *Adsorption* **2016**, *22*, 261–276. [CrossRef]

70. Zhou, Y.; Zhang, R.; Huang, J.; Li, Z.; Zhao, Z.; Zeng, Z. Effects of pore structure and methane adsorption in coal with alkaline treatment. *Fuel* **2019**, *254*, 115600. [CrossRef]

71. Bakshi, T.; Prusty, B.; Pathak, K.; Nayak, B.; Mani, D.; Pal, S. Source rock characteristics and pore characterization of Indian shale. *J. Nat. Gas Sci. Eng.* **2017**, *45*, 761–770. [CrossRef]

72. Qin, L.; Li, S.; Zhai, C.; Lin, H.; Zhao, P.; Yan, M.; Ding, Y.; Shi, Y. Joint analysis of pores in low, intermediate, and high rank coals using mercury intrusion, nitrogen adsorption, and nuclear magnetic resonance. *Powder Technol.* **2020**, *362*, 615–627. [CrossRef]

73. Li, S.; Tang, D.; Xu, H.; Yang, Z. The pore-fracture system properties of coalbed methane reservoirs in the Panguan Syncline, Guizhou, China. *Geosci. Front.* **2012**, *3*, 853–862. [CrossRef]

74. Li, Z.; Liu, D.; Cai, Y.; Wang, Y.; Teng, J. Adsorption pore structure and its fractal characteristics of coals by N2 adsorption/desorption and FESEM image analyses. *Fuel* **2019**, *257*, 116031. [CrossRef]

75. Clarkson, C.; Bustin, R. The effect of pore structure and gas pressure upon the transport properties of coal: A laboratory and modeling study. 1. Isotherms and pore volume distributions. *Fuel* **1999**, *78*, 1333–1344. [CrossRef]

76. Parkash, S.; Chakrabartty, S. Microporosity in Alberta Plains coals. *Int. J. Coal Geol.* **1986**, *6*, 55–70. [CrossRef]

77. Sun, W.; Feng, Y.; Jiang, C.; Chu, W. Fractal characterization and methane adsorption features of coal particles taken from shallow and deep coalmine layers. *Fuel* **2015**, *155*, 7–13. [CrossRef]

78. Yao, Y.; Liu, D. Effects of igneous intrusions on coal petrology, pore-fracture and coalbed methane characteristics in Hongyang, Handan and Huaibei coalfields, North China. *Int. J. Coal Geol.* **2012**, *96–97*, 72–81. [CrossRef]

79. Staib, G.; Sakurovs, R.; Gray, E.M.A. A pressure and concentration dependence of CO_2 diffusion in two Australian bituminous coals. *Int. J. Coal Geol.* **2013**, *116–117*, 106–116. [CrossRef]

80. Zhou, Y.; Li, Z.; Zhang, R.; Wang, G.; Yu, H.; Sun, G.; Chen, L. CO_2 injection in coal: Advantages and influences of temperature and pressure. *Fuel* **2018**, *236*, 493–500. [CrossRef]

81. Yamazaki, T.; Aso, K.; Chinju, J. Japanese potential of CO_2 sequestration in coal seams. *Appl. Energy* **2006**, *83*, 911–920. [CrossRef]

82. Busch, A.; Gensterblum, Y.; Krooss, B.M. High-Pressure Sorption of Nitrogen, Carbon Dioxide, and their Mixtures on Argonne Premium Coals. *Energy Fuels* **2007**, *21*, 1640–1645. [CrossRef]

83. Cui, X.; Bustin, R.; Dipple, G. Selective transport of CO_2, CH_4, and N_2 in coals: Insights from modeling of experimental gas adsorption data. *Fuel* **2004**, *83*, 293–303. [CrossRef]

84. Zheng, G.; Pan, Z.; Tang, S.; Ling, B.; Lv, D.; Connell, L.D. Laboratory and Modeling Study on Gas Diffusion with Pore Structures in Different-Rank Chinese Coals. *Energy Explor. Exploit.* **2013**, *31*, 859–877. [CrossRef]

85. Bhowmik, S.; Dutta, P. Adsorption rate characteristics of methane and CO_2 in coal samples from Raniganj and Jharia coalfields of India. *Int. J. Coal Geol.* **2013**, *113*, 50–59. [CrossRef]

86. Charrière, D.; Pokryszka, Z.; Behra, P. Effect of pressure and temperature on diffusion of CO_2 and CH_4 into coal from the Lorraine basin (France). *Int. J. Coal Geol.* **2010**, *81*, 373–380. [CrossRef]

87. Zhao, J.; Tang, D.; Qin, Y.; Xu, H.; Liu, Y.; Wu, H. Characteristics of Methane (CH_4) Diffusion in Coal and Its Influencing Factors in the Qinshui and Ordos Basins. *Energy Fuels* **2018**, *32*, 1196–1205. [CrossRef]

88. Li, X.; Yan, X.; Kang, Y. Effect of temperature on the permeability of gas adsorbed coal under triaxial stress conditions. *J. Geophys. Eng.* **2017**, *15*, 386–396. [CrossRef]

89. Fang, H.; Sang, S.; Liu, S. The coupling mechanism of the thermal-hydraulic-mechanical fields in CH4-bearing coal and its application in the CO_2-enhanced coalbed methane recovery. *J. Pet. Sci. Eng.* **2019**, *181*, 106177. [CrossRef]

90. Wang, X.; Zhang, D.; Su, E.; Jiang, Z.; Wang, C.; Chu, Y.; Ye, C. Pore structure and diffusion characteristics of intact and tectonic coals: Implications for selection of CO_2 geological sequestration site. *J. Nat. Gas Sci. Eng.* **2020**, *81*, 103388. [CrossRef]

91. Dutta, A. Multicomponent Gas Diffusion and Adsorption in Coals for Enhanced Methane Recovery. Master's Thesis, Stanford University, Stanford, USA, June 2009.

92. Abunowara, M.; Sufian, S.; Bustam, M.A.; Eldemerdash, U.; Suleman, H.; Bencini, R.; Assiri, M.A.; Ullah, S.; Al-Sehemi, A.G. Experimental measurements of carbon dioxide, methane and nitrogen high-pressure adsorption properties onto Malaysian coals under various conditions. *Energy* **2020**, *210*, 118575. [CrossRef]

93. George, J.S.; Barakat, M. The change in effective stress associated with shrinkage from gas desorption in coal. *Int. J. Coal Geol.* **2001**, *45*, 105–113. [CrossRef]

94. Joewondo, N. Pore Sturucture of Micro and Mesoporous Mudrocks Based on Nitrogen and Carbon Sorption. Master's Thesis, Colorado School of Mines, Golden, Colorado, 2018.

95. Aleghafouri, A.; Mohsen-Nia, M.; Mohajeri, A.; Mahdyarfar, M.; Asghari, M. Micropore Size Analysis of Activated Carbons Using Nitrogen, Carbon Dioxide and Methane Adsorption Isotherms: Experimental and Theoretical Studies. *Adsorpt. Sci. Technol.* **2012**, *30*, 307–316. [CrossRef]

96. Wang, H.; Fu, X.; Jian, K.; Li, T.; Luo, P. Changes in coal pore structure and permeability during N 2 injection. *J. Nat. Gas Sci. Eng.* **2015**, *27*, 1234–1241. [CrossRef]

97. Fang, Z.; Li, X.; Hu, H. Gas mixture enhance coalbed methane recovery technology: Pilot tests. *Energy Procedia* **2011**, *4*, 2144–2149. [CrossRef]

98. Reeves, S. The Coal-Seq Project: Key Results from Field, Laboratory, and Modeling Studies. *Greenh. Gas Control Technol.* **2005**, *II*, 1399–1403.

99. Zhu, H.; He, X.; Xie, Y.; Guo, S.; Huo, Y.; Wang, W. A Study on the Effect of Coal Metamorphism on the Adsorption Characteristics of a Binary Component System: CO_2 and N_2. *ACS Omega* **2020**, *6*, 523–532. [CrossRef]

100. Zhang, L.; Aziz, N.; Ren, T.X.; Wang, Z. Influence of Temperature on Coal Sorption Characteristics and the Theory of Coal Surface Free Energy. *Procedia Eng.* **2011**, *26*, 1430–1439. [CrossRef]

101. Hao, M.; Qiao, Z.; Zhang, H.; Wang, Y.; Li, Y. Thermodynamic Analysis of $CH_4/CO_2/N_2$ Adsorption on Anthracite Coal: Investigated by Molecular Simulation. *Energy Fuels* **2021**, *35*, 4246–4257. [CrossRef]
102. Romanov, V.; Soong, Y.; Schroeder, K. Volumetric Effects in Coal Sorption Capacity Measurements. *Chem. Eng. Technol.* **2006**, *29*, 368–374. [CrossRef]
103. Day, S.; Duffy, G.; Saghafi, A.; Sakurovs, R. Factors controlling CO_2 absorption in Australian coals. *Greenh. Gas Control. Technol.* **2005**, *2*, 2519–2523. [CrossRef]
104. Sudibandriyo, M.; Pan, Z.; Fitzgerald, J.E.; Robinson, R.L.; Gasem, K.A.M. Adsorption of Methane, Nitrogen, Carbon Dioxide, and Their Binary Mixtures on Dry Activated Carbon at 318.2 K and Pressures up to 13.6 MPa. *Langmuir* **2003**, *19*, 5323–5331. [CrossRef]
105. De Weireld, G.; Frere, M.; Jadot, R. Automated determination of high-temperature and high-pressure gas adsorption isotherms using a magnetic suspension balance. *Meas. Sci. Technol.* **1999**, *10*, 117–126. [CrossRef]
106. Zhang, Y.; Xing, W.; Liu, S.; Liu, Y.; Yang, M.; Zhao, J.; Song, Y. Pure methane, carbon dioxide, and nitrogen adsorption on anthracite from China over a wide range of pressures and temperatures: Experiments and modeling. *RSC Adv.* **2015**, *5*, 52612–52623. [CrossRef]
107. Du, X.; Cheng, Y.; Liu, Z.; Yin, H.; Wu, T.; Huo, L.; Shu, C. CO_2 and CH_4 adsorption on different rank coals: A thermodynamics study of surface potential, Gibbs free energy change and entropy loss. *Fuel* **2021**, *283*, 118886. [CrossRef]
108. Deng, J.; Kang, J.; Zhou, F.; Li, H.; Zhang, D.; Li, G. The adsorption heat of methane on coal: Comparison of theoretical and calorimetric heat and model of heat flow by microcalorimeter. *Fuel* **2019**, *237*, 81–90. [CrossRef]
109. Liu, X.-Q.; He, X.; Qiu, N.-X.; Yang, X.; Tian, Z.-Y.; Li, M.-J.; Xue, Y. Molecular simulation of CH_4, CO_2, H_2O and N_2 molecules adsorption on heterogeneous surface models of coal. *Appl. Surf. Sci.* **2016**, *389*, 894–905. [CrossRef]
110. Clarkson, C.; Bustin, R.; Levy, J. Application of the mono/multilayer and adsorption potential theories to coal methane adsorption isotherms at elevated temperature and pressure. *Carbon* **1997**, *35*, 1689–1705. [CrossRef]
111. Kumar, A. Adsorption of Methane on Activated Carbon by Volumetric Method. *Chem. Eng.* **2011**. [CrossRef]
112. Langmuir, I. The adsorption of gases on plane surfaces of glass, mica and platinum. *J. Am. Chem. Soc.* **1918**, *40*, 1361–1403. [CrossRef]
113. Adams, J.J. Asphaltene Adsorption, a Literature Review. *Energy Fuels* **2014**, *28*, 2831–2856. [CrossRef]
114. Montoya, T.; Coral, D.; Franco, C.A.; Nassar, N.N.; Cortés, F.B. A Novel Solid–Liquid Equilibrium Model for Describing the Adsorption of Associating Asphaltene Molecules onto Solid Surfaces Based on the "Chemical Theory". *Energy Fuels* **2014**, *28*, 4963–4975. [CrossRef]
115. Keller, J.U.; Staudt, R. *Gas Adsorption Equilibria: Experimental Methods and Adsorptive Isotherms*; Springer: Berlin/Heidelberg, Germany, 2005; ISBN 0387235981.
116. Zhao, J.; Xu, H.; Tang, D.; Mathews, J.P.; Li, S.; Tao, S. A comparative evaluation of coal specific surface area by CO_2 and N_2 adsorption and its influence on CH_4 adsorption capacity at different pore sizes. *Fuel* **2016**, *183*, 420–431. [CrossRef]
117. Zhu, Q.; Yang, Y.; Lu, X.; Liu, D.; Li, X.; Zhang, Q.; Cai, Y. Pore Structure of Coals by Mercury Intrusion, N_2 Adsorption and NMR: A Comparative Study. *Appl. Sci.* **2019**, *9*, 1680. [CrossRef]
118. Masoudian, M.S. Multiphysics of carbon dioxide sequestration in coalbeds: A review with a focus on geomechanical characteristics of coal. *J. Rock Mech. Geotech. Eng.* **2016**, *8*, 93–112. [CrossRef]
119. Liu, Z.; Zhang, Z.; Choi, S.K.; Lu, Y. Surface Properties and Pore Structure of Anthracite, Bituminous Coal and Lignite. *Energies* **2018**, *11*, 1502. [CrossRef]
120. Clarkson, C.R.; Bustin, R.M. Variation in micropore capacity and size distribution with composition in bituminous coal of the Western Canadian Sedimentary Basin: Implications for coalbed methane potential. *Fuel* **1996**, *75*, 1483–1498. [CrossRef]
121. Landers, J.; Gor, G.Y.; Neimark, A.V. Density functional theory methods for characterization of porous materials. *Colloids Surf. A Physicochem. Eng. Asp.* **2013**, *437*, 3–32. [CrossRef]
122. Thommes, M. Pore Size Analysis by Gas Adsorption Part I: Aspects of the Application of Density Functional Theory (DFT) and Monte Carlo Simulation (MC) for Micro/Mesopore Size Analysis. Available online: http://www.quantachrome.com/articles.html (accessed on 9 November 2020).
123. Seaton, N.A.; Walton, J.P.R.B.; Quirke, N. A new analysis method for the determination of the pore size distribution of porous carbons from nitrogen adsorption measurements. *Carbon* **1989**, *27*, 853–861. [CrossRef]
124. Zhang, J.; Liu, K.; Clennell, M.; Dewhurst, D.; Pervukhina, M. Molecular simulation of CO_2–CH_4 competitive adsorption and induced coal swelling. *Fuel* **2015**, *160*, 309–317. [CrossRef]
125. Gao, D.; Hong, L.; Wang, J.; Zheng, D. Adsorption simulation of methane on coals with different metamorphic grades. *AIP Adv.* **2019**, *9*, 095108. [CrossRef]
126. Yang, Z.; Yin, Z.; Xue, W.; Meng, Z.; Li, Y.; Long, J.; Wang, J. Construction of Buertai Coal Macromolecular Model and GCMC Simulation of Methane Adsorption in Micropores. *ACS Omega* **2021**, *6*, 11173–11182. [CrossRef]
127. He, X.; Liu, X.; Nie, B.; Song, D. FTIR and Raman spectroscopy characterization of functional groups in various rank coals. *Fuel* **2017**, *206*, 555–563. [CrossRef]
128. Maphala, T.; Wagner, N.J. Effects of CO_2 storage in coal on coal properties. *Energy Procedia* **2012**, *23*, 426–438. [CrossRef]
129. Zuo, P.; Qu, S.; Shen, W. Asphaltenes: Separations, structural analysis and applications. *J. Energy Chem.* **2019**, *34*, 186–207. [CrossRef]

130. Wang, J.; He, Y.; Li, H.; Yu, J.; Xie, W.; Wei, H. The molecular structure of Inner Mongolia lignite utilizing XRD, solid state 13C NMR, HRTEM and XPS techniques. *Fuel* **2017**, *203*, 764–773. [CrossRef]

131. Perera, S.; Ranjith, P.; Viete, D. Effects of gaseous and super-critical carbon dioxide saturation on the mechanical properties of bituminous coal from the Southern Sydney Basin. *Appl. Energy* **2013**, *110*, 73–81. [CrossRef]

132. Syed, A.; Durucan, S.; Shi, J.-Q.; Korre, A. Flue Gas Injection for CO_2 Storage and Enhanced Coalbed Methane Recovery: Mixed Gas Sorption and Swelling Characteristics of Coals. *Energy Procedia* **2013**, *37*, 6738–6745. [CrossRef]

133. Pirzada, M.A.; Zoorabadi, M.; Ramandi, H.L.; Canbulat, I.; Roshan, H. CO_2 sorption induced damage in coals in unconfined and confined stress states: A micrometer to core scale investigation. *Int. J. Coal Geol.* **2018**, *198*, 167–176. [CrossRef]

134. Levine, J.R. Model study of the influence of matrix shrinkage on absolute permeability of coal bed reservoirs. *Geol. Soc. Lond. Spéc. Publ.* **1996**, *109*, 197–212. [CrossRef]

135. Anggara, F.; Sasaki, K.; Sugai, Y. The correlation between coal swelling and permeability during CO 2 sequestration: A case study using Kushiro low rank coals. *Int. J. Coal Geol.* **2016**, *166*, 62–70. [CrossRef]

136. Niu, Y.; Mostaghimi, P.; Shikhov, I.; Chen, Z.; Armstrong, R.T. Coal permeability: Gas slippage linked to permeability rebound. *Fuel* **2018**, *215*, 844–852. [CrossRef]

137. Zhang, B.; Zhu, J.; Tang, D.; Jiang, Y. The effect of adsorption-induced swelling on porosity based on the transient coal swelling model. *AIP Adv.* **2019**, *9*, 035229. [CrossRef]

138. Day, S.; Fry, R.; Sakurovs, R.; Weir, S. Swelling of Coals by Supercritical Gases and Its Relationship to Sorption. *Energy Fuels* **2010**, *24*, 2777–2783. [CrossRef]

139. Chen, G.; Yang, J.; Liu, Z. Method for Simultaneous Measure of Sorption and Swelling of the Block Coal under High Gas Pressure. *Energy Fuels* **2012**, *26*, 4583–4589. [CrossRef]

140. Wang, G.; Wei, X.; Wang, K.; Massarotto, P.; Rudolph, V. Sorption-induced swelling/shrinkage and permeability of coal under stressed adsorption/desorption conditions. *Int. J. Coal Geol.* **2010**, *83*, 46–54. [CrossRef]

141. Anggara, F.; Sasaki, K.; Sugai, Y. Mineral Dissolution/Precipitation during CO_2 Injection into Coal Reservoir: A Laboratory Study. *Energy Procedia* **2013**, *37*, 6722–6729. [CrossRef]

142. Mastalerz, M.; Goodman, A.; Chirdon, D. Coal Lithotypes before, during, and after Exposure to CO_2: Insights from Direct Fourier Transform Infrared Investigation. *Energy Fuels* **2012**, *26*, 3586–3591. [CrossRef]

143. Baysal, M.; Yürüm, A.; Yıldız, B.; Yürüm, Y. Structure of some western Anatolia coals investigated by FTIR, Raman, 13C solid state NMR spectroscopy and X-ray diffraction. *Int. J. Coal Geol.* **2016**, *163*, 166–176. [CrossRef]

144. Cao, X.; Mastalerz, M.; Chappell, M.A.; Miller, L.F.; Li, Y.; Mao, J. Chemical structures of coal lithotypes before and after CO_2 adsorption as investigated by advanced solid-state 13C nuclear magnetic resonance spectroscopy. *Int. J. Coal Geol.* **2011**, *88*, 67–74. [CrossRef]

145. Wang, K.; Du, F.; Wang, G. The influence of methane and CO 2 adsorption on the functional groups of coals: Insights from a Fourier transform infrared investigation. *J. Nat. Gas Sci. Eng.* **2017**, *45*, 358–367. [CrossRef]

146. Mastalerz, M.; Drobniak, A.; Walker, R.; Morse, D. Coal lithotypes before and after saturation with CO_2; insights from micro- and mesoporosity, fluidity, and functional group distribution. *Int. J. Coal Geol.* **2010**, *83*, 467–474. [CrossRef]

147. Zhang, J.; Wei, C.; Zhao, C.; Zhang, T.; Lu, G.; Zou, M. Effects of nano-pore and macromolecule structure of coal samples on energy parameters variation during methane adsorption under different temperature and pressure. *Fuel* **2021**, *289*, 119804. [CrossRef]

148. Sonibare, O.O.; Haeger, T.; Foley, S. Structural characterization of Nigerian coals by X-ray diffraction, Raman and FTIR spectroscopy. *Energy* **2010**, *35*, 5347–5353. [CrossRef]

149. Pan, J.; Lv, M.; Hou, Q.; Han, Y.; Wang, K. Coal microcrystalline structural changes related to methane adsorption/desorption. *Fuel* **2019**, *239*, 13–23. [CrossRef]